




An experimental study of a two-degree-of-freedom galloping energy harvester

Guobiao Hu^{1,3}  | Junlei Wang^{1,2,3}  | Hongwei Qiao² | Liya Zhao⁴  |
Zhaoyu Li³ | Lihua Tang³ 

¹Engineering Research Center of Energy Saving Technology and Equipment of Thermal Energy System, Ministry of Education, Zhengzhou University, Zhengzhou, China

²School of Mechanical and Power Engineering, Zhengzhou University, Zhengzhou, China

³Department of Mechanical Engineering, University of Auckland, Auckland, New Zealand

⁴School of Mechanical and Mechatronic Engineering, Faculty of Engineering and Information Technology, University of Technology Sydney, Ultimo, New South Wales, Australia

Correspondence

Junlei Wang and Lihua Tang, Department of Mechanical Engineering, University of Auckland, Auckland, New Zealand.
Email: jlwang@zsu.edu.cn (J. Wang);
l.tang@auckland.ac.nz (L. Tang)

Funding information

National Natural Science Foundation of China

Summary

The cut-in wind speed and the power output are the two main concerns of a galloping energy harvester. A good galloping energy harvester is expected to have a low cut-in wind speed and a high power output. This paper proposes a two-degree-of-freedom (2-DOF) galloping-based piezoelectric energy harvester (GPEH) by mounting a secondary beam onto a primary piezoelectric cantilever beam. An experimental study is conducted to evaluate the actual energy harvesting performance of the proposed 2-DOF GPEH. The effects of the secondary beam length and the mounting position on the cut-in wind speed and the power output are investigated. It is revealed that the introduction of the secondary beam can reduce the cut-in wind speed from 2.372 m/s to 1.961 m/s. Mounting the secondary beam further away from the bluff body weakens the influence of the secondary beam on the energy harvesting performance of the 2-DOF GPEH. Moreover, the power output can be increased or decreased by tuning the secondary beam length. The power output from a well-tuned 2-DOF GPEH can be increased for about 111.1%, as compared to the conventional 1-DOF GPEH. By contrast, the power output from a badly tuned 2-DOF GPEH is reduced for about 22.2%. A simple theoretical model is developed for explaining the experimentally observed phenomenon and can be used to provide some guidelines in the design of 2-DOF GPEH to avoid performance deterioration.

1 | INTRODUCTION

Harvesting energy from ubiquitous wind¹⁻³ has been extensively studied for the purpose to power micro-electro-mechanical systems (MEMS)⁴⁻¹¹ in the past decade. The development of wind energy harvesters requires to convert wind energy into structural vibration energy first using various flow-induced vibration mechanisms,¹²⁻¹⁵ such as galloping,¹⁶⁻¹⁸ wake galloping,^{19,20} flutter²¹ and vortex-induced vibration.²²⁻²⁵ To subsequently convert vibration energy into electricity, there are several energy transduction methods including electromagnetic,²⁶⁻²⁹

electrostatic^{30,31} and piezoelectric effects.³²⁻³⁶ Because of the advantage of high-power density, using piezoelectric materials for energy harvesting has attracted numerous research interests. On the other hand, to broaden the bandwidth or improve the energy harvesting efficiency, various innovative mechanical structures have been proposed.³⁷⁻⁴⁰

Due to the characteristics of large oscillation amplitudes and a wide range of operating wind speed, galloping-based piezoelectric energy harvesters (GPEHs) have been explosively researched. A typical GPEH can be obtained by attaching a bluff body to the free end of a

piezoelectric beam.⁴¹ Due to the wind-structure interaction, a lift force is applied onto the bluff body with an asymmetrical conductor profile. The lift force is perpendicular to the wind speed and behaves like a negative damping term which is the key to incurring the self-excited vibration of the system. A GPEH is often modelled as a one-degree-of-freedom (1-DOF) system and mathematically described by lumped parameters.⁴² On the basis of the 1-DOF model, Tang et al⁴³ and Wang et al⁴⁴ established an equivalent circuit model (ECM) to enable the analysis of a GPEH and VIVPEH shunted to various complicated interface circuits. Yang et al³³ compared the performance of a GPEH using bluff bodies with different cross-sections and concluded that a square-sectioned bluff body yielded the best energy harvesting performance.

Besides the fundamental research, some researchers explored various innovative configurations to improve the performance of GPEHs. Bibo et al,⁴⁵ Yang et al,⁴⁶ and Wang et al⁴⁷ proposed bistable or tristable GPEHs by introducing a magnetic nonlinearity to improve the energy harvesting performance. It was found that the inter-well oscillation enabled the nonlinear GPEHs to achieve enhanced power outputs. Yang et al⁴⁶ and Wang et al⁴⁸ employed a double-beam system in the design of a novel galloping energy harvester. The experimental results showed that the cut-in wind speed of the proposed double-beam GPEH could be significantly reduced up to 41.9%. He et al⁴⁹ enhanced the performance of a wind energy harvesting by the interaction between vortex-induced vibration and galloping. Wang et al⁵⁰ proposed to add Y-shaped attachments on the bluff body, which resulted in the transition from vortex-induced vibrations into galloping and thus the energy harvesting performance enhancement. Instead of using the conventional 1-DOF design for galloping energy harvesting, Zhao et al⁵¹ proposed a nonlinear 2-DOF GPEH based on a cut-out cantilever beam. The experimental results showed that the cut-in wind speed was beneficially decreased and the power output was increased. Sun et al⁵² also developed a 2-DOF GPEH based on a nested structure. It was experimentally observed that the proposed 2-DOF GPEH exhibited an enhanced power output. Recently, Lan et al⁵³ conducted a comprehensive theoretical study of two configurations of a 2-DOF GPEH using the harmonic balance method. The effects of the systems parameters on the energy harvesting performance were investigated. According to the state of the art, the research on 2-DOF GPEH is still in its infancy. Though Lan et al⁵³ presented a comprehensive theoretical study, there lacks any experimental insight into the actual performance of a physically prototyped 2-DOF GPEH. This paper presents the design of a 2-DOF GPEH

and focuses on the experimental study. A mode-activation phenomenon is observed and reported for the first time. A simple theoretical model is developed and a qualitative analysis is provided to explain the phenomenon observed in the experiment.

2 | PHYSICAL PROTOTYPE

Figure 1(A) shows the schematic of the proposed galloping energy harvester. Such kind of system can be regarded as a 2-DOF system,⁵⁴ which is the reason why we term it as a 2-DOF GPEH. One end of the primary beam is clamped and the other end is attached with a cuboid bluff body. The primary beam is made of aluminium with the length, width and thickness of 140 mm, 20 mm and 0.5 mm, respectively. The design criterion for a galloping energy harvester is that the fundamental natural frequency should not be very high. Otherwise, the cut-in wind speed will be very high, making it difficult for low-speed wind energy harvesting. According to this design criterion, it is not essential to use aluminium to make the primary beam. One can use other materials, such as steel, to make a primary beam as long as proper dimensions are chosen to achieve a low natural frequency. However, it is obvious that using aluminium material is easier to lower the fundamental natural frequency because of its relatively low Young's modulus. Due to this practical reason, we used the aluminium material to make the primary beam. A macro fibre composite (MFC) patch (Model: 2814P2, Smart Material Corp., Germany) is bonded at the clamped root of the primary beam for power generation. The bluff body is made of foam with the geometric dimensions of $140 \times 32 \times 32 \text{ mm}^3$ and the mass density of 16 kg/m^3 . A secondary steel beam is symmetrically mounted onto the primary beam by screw connection. For the secondary beam, it is not essential to use the steel material, either. From the theoretical point of view, one can use other materials such as aluminium, bronze, etc. The design criterion for the secondary beam is that during the vibration, plastic deformation should not take place in the secondary beam. According to the theory of the dynamic amplifier, the vibration amplitude of the secondary beam could be much larger than the primary beam. Thus, plastic deformation could more easily occur in the secondary beam. For this reason, we used steel rather than aluminium to make the secondary beam, as steel material has a higher yield strength. However, we need to state that with proper geometric dimensions, one can use other materials to satisfy the same design criterion. The secondary beam is actually split into two identical small cantilever beams. This symmetric design is to ensure that the motions of the two identical

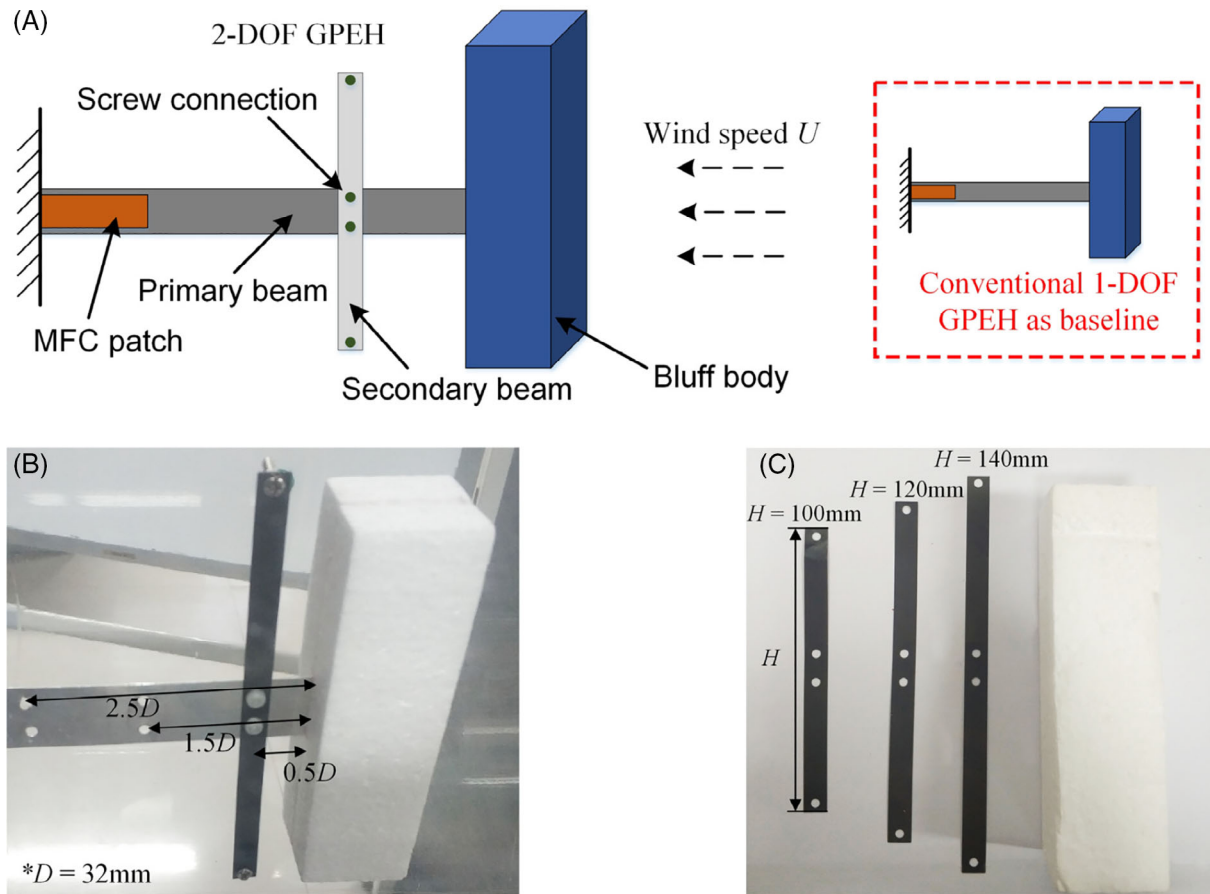


FIGURE 1 (A) Schematic diagram of the proposed 2-DOF GPEH and the conventional 1-DOF GPEH as baseline, (B) three sets of mounting positions, (C) three sets of secondary beams with different lengths [Colour figure can be viewed at wileyonlinelibrary.com]

small cantilever beams are exactly the same to avoid torsional motion of the primary beam caused by imbalance. For a symmetric design, there also exist torsional vibration modes. However, when the external load is symmetrically applied, for example, the current uniform wind load that is evenly distributed over the bluff body, the torsional vibration modes with asymmetric shapes cannot be stimulated. In fact, when the secondary beam is relatively small and lighter as compared to the host beam. Even without the symmetric design, the torsional vibration modes exist in the high frequency range and its influence on the dynamic motion around the fundamental resonance is very minor. An example study of an asymmetric design without evident torsional vibration influence in the low frequency regime can be found in.⁵⁵ On the other hand, when the secondary beam is relatively heavy, an asymmetric design results in a non-ignorable imbalance. The torsional vibration mode will appear in the low-frequency range and has a significant influence on the fundamental vibration mode shape. A relevant study can be found in.⁵⁶ The condition for the appearance of an evident torsional vibration in an asymmetric design is actually different for

different systems. In the current study, for simplicity, we intentionally adopt the symmetric design strategy to certainly obviate the torsional vibration. The width and thickness of the secondary beam are 8 mm and 0.1 mm, respectively. A pair of nut and bolt with the total mass of 1.8 g is attached to each free end of the secondary beam to serve as the tip mass. Three sets of screw holes are drilled on the primary beam to enable the change of the mounting position of the secondary beam (as shown in Figure 1 (B)). Moreover, three sets of secondary beams with different lengths (100, 120 and 140 mm) are prepared to be tested (as shown in Figure 1c). It is worth mentioning that a conventional 1-DOF GPEH is obtained by directly removing the secondary beam.

In the experiment, the physical prototype is installed in a circular wind tunnel with the cross-sectional diameter of 0.4 m. By controlling the rotating speed of a draught fan, different wind speeds can be produced. The honey comb is used to stabilize the air flow in the tunnel. The digital oscilloscope (Model: DS1104S, RIGOL., China) is used to acquire the voltage output of the piezoelectric transducer.

3 | RESULTS AND DISCUSSIONS

To investigate the effects of introducing the secondary beam on the cut-in wind speed, the open-circuit voltage outputs vs the wind speed for the proposed 2-DOF GPEH are plotted in Figure 2. The result for the conventional 1-DOF GPEH is also provided for comparison. The cut-in wind speed of the conventional 1-DOF GPEH is 2.372 m/s. Figure 2(A) shows the result of using a secondary beam with the length $H = 100$ mm. It can be noted that adding the secondary beam to the primary significantly reduces the cut-in wind speed. By mounting the secondary beam at a distance of $0.5D$ from the bluff body, the cut-in wind speed is reduced from 2.372 m/s to 1.961 m/s. Moreover, the open-circuit voltage output is significantly increased for the full range of wind speed. For instance, at the wind speed of 3.605 m/s, the voltage of the 2-DOF GPEH with the $0.5D$ configuration is about 27.11 V, which indicates a 52.3% increase as compared to the conventional 1-DOF GPEH (17.80 V). It is also found that the improvement brought by the secondary beam becomes smaller when the secondary beam is mounted further away from the bluff body. At a distance of $2.5D$, the enhancement is negligible and the performance of the 2-DOF GPEH becomes similar to that of the 1-DOF GPEH.

Figure 2(B) and C shows the results of two more cases with the secondary beam length being increased to 120 and 140 mm, respectively. The increase of the secondary beam length implies the decrease of its natural frequency. For $H = 120$ mm, improvements brought by the secondary beam can still be observed: the cut-in wind speed is reduced and the open-circuit voltage amplitude is increased. However, for $H = 140$ mm, except when the secondary beam is mounted at the distance of $0.5D$ from

the bluff body, the cut-in wind speed of the 2-DOF GPEH is almost the same as that of the 1-DOF GPEH. In terms of the open-circuit voltage, in contrast to previous cases, the amplitude of the 2-DOF GPEH is slightly decreased as compared to the 1-DOF GPEH.

Figure 3(A)-C shows the output power vs electrical resistance for the 2-DOF GPEH with a secondary beam of different lengths under different wind speeds. It is found that the optimal resistances for all the cases are nearly the same: $R_{optimal}$ is around 500 k Ω . Therefore, it can be concluded that the optimal resistance is only dependent on the primary structure. For a given wind speed $U = 3.47$ m/s, the optimal power outputs from the 2-DOF GPEH with the secondary beam length of 100 mm, 120 mm and 140 mm are 0.57 mW, 0.51 mW and 0.21 mW, respectively. Under the same wind speed, the optimal power output from the 1-DOF GPEH is about 0.27 mW. It can be found that as predicted from the open-circuit voltage analysis, the configurations of $H = 100$ mm and $H = 120$ mm show better performance as compared to the 1-DOF GPEH, while the power output from the configuration of $H = 140$ mm is slightly reduced. With $H = 100$ mm, a power enhancement of 111.1% is achieved.

To help understand the working mechanism, a simple theoretical model is presented. The primary DOF denotes the host beam together with the bluff body and the secondary DOF represents the secondary beam with the tip mass. m_1 is the equivalent mass of the host beam together with the bluff body and k_1 is the equivalent stiffness of the host beam. Similarly, m_2 is the equivalent mass of the secondary beam with the tip mass and k_2 is the equivalent stiffness of the secondary beam. Neglecting the damping terms and omitting the electromechanical

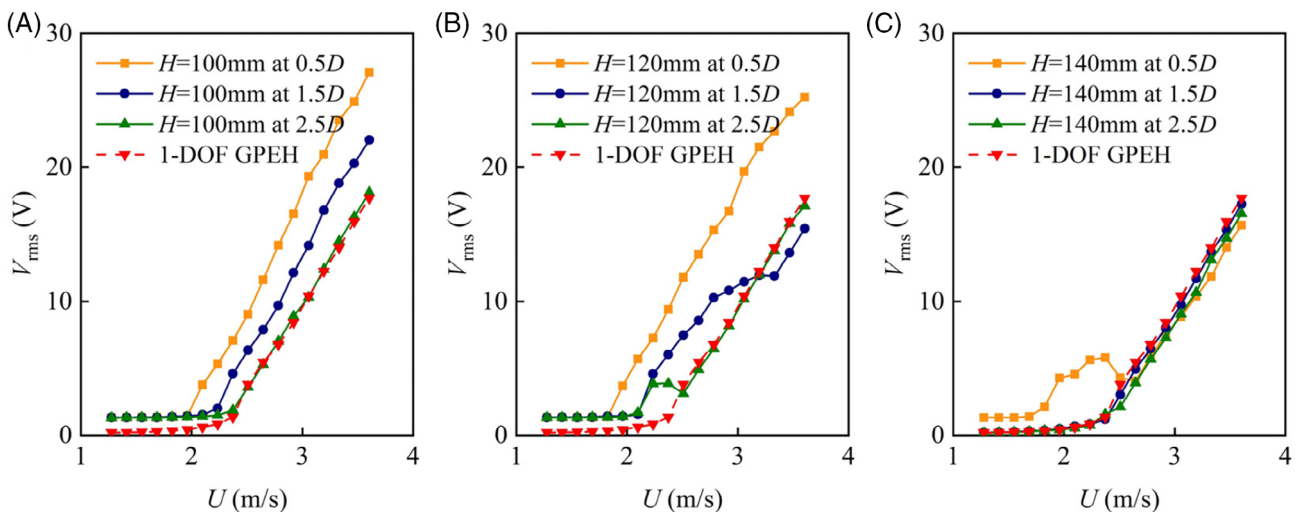


FIGURE 2 Open-circuit voltage vs wind speed for the proposed 2-DOF GPEH with a secondary beam of the length (A) $H = 100$ mm, (B) $H = 120$ mm, (C) $H = 140$ mm. The subscript rms denotes the root mean square [Colour figure can be viewed at wileyonlinelibrary.com]

coupling effect, the two natural frequencies of the coupled 2-DOF system as shown in Figure 4(A) are:

$$\begin{cases} \omega_1 = \frac{1}{2} \left[\omega_{1,0}^2 + (\mu + 1)\omega_{2,0}^2 - \sqrt{\omega_{1,0}^4 + 2(\mu - 1)\omega_{1,0}^2\omega_{2,0}^2 + (\mu + 1)^2\omega_{2,0}^4} \right] \\ \omega_2 = \frac{1}{2} \left[\omega_{1,0}^2 + (\mu + 1)\omega_{2,0}^2 + \sqrt{\omega_{1,0}^4 + 2(\mu - 1)\omega_{1,0}^2\omega_{2,0}^2 + (\mu + 1)^2\omega_{2,0}^4} \right] \end{cases} \quad (1)$$

where $\mu = \frac{m_2}{m_1}$, $\omega_{1,0} = \sqrt{k_1/m_1}$, $\omega_{2,0} = \sqrt{k_2/m_2}$. It can be proved that the natural frequencies of the coupled 2-DOF system are the solutions to the frequency of dynamic response of the 2-DOF GPEH.⁵³ In addition, it can be proved that the two DOFs have in-phase motion around the first mode and out-of-phase motion around the second mode. Figure 4(B) shows the relationship between the natural frequencies of the coupled 2-DOF system (ie, ω_1 & ω_2) and the natural frequencies of the two standalone systems

(ie, $\omega_{1,0}$ & $\omega_{2,0}$). The two curves representing ω_1 and ω_2 are similar to two branches of a hyperbola. The dimensionless parameter μ determines the radius of curvature. It can be seen that $\omega_1 < \min(\omega_{1,0}, \omega_{2,0})$ and $\omega_2 > \max(\omega_{1,0}, \omega_{2,0})$. Moreover, it is worth noting that when $\omega_{2,0}$ is small, $\omega_1 \approx \omega_{2,0}$ and $\omega_2 \approx \omega_{1,0}$. The physical meaning is that when the k_2 is small, the coupling between the primary and the secondary systems becomes weak and the two systems are almost uncoupled, operating nearly independently.

As the aerodynamic force is directly applied onto the primary system, it can be expected that regardless of the tuning of the secondary system, the dynamic motion of the primary system can be induced at a frequency around $\omega_{1,0}$ once the wind speed exceeds the threshold value. It can be deduced that when $\omega_{2,0}$ is tuned smaller than $\omega_{1,0}$, the second vibration mode of the coupled 2-DOF might be stimulated by the self-excited oscillation, since $\|\omega_{1,0} - \omega_2\| < \|\omega_{1,0} - \omega_1\|$ ($\|\cdot\|$ denotes the Euclidean distance). In this case, since the

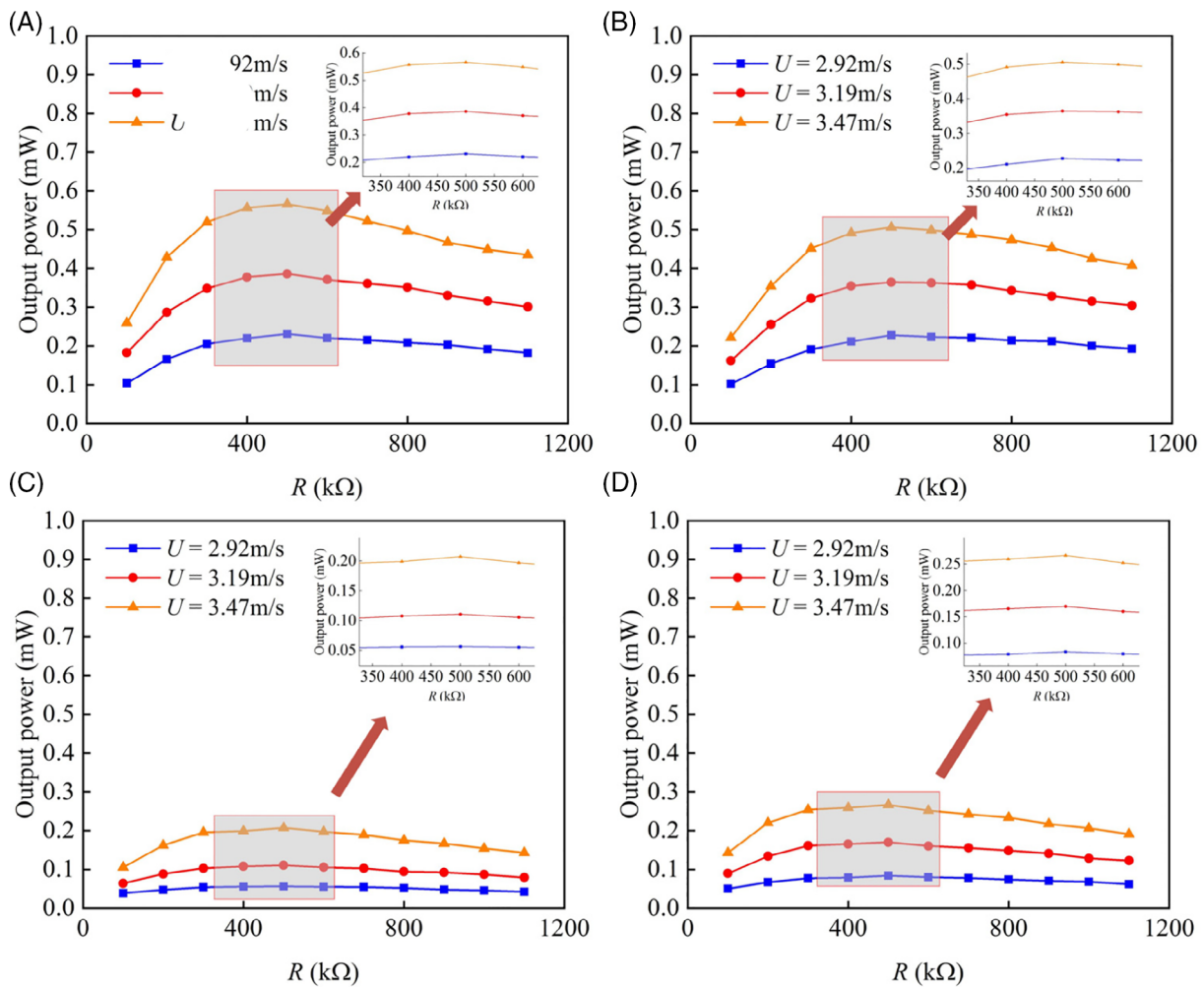


FIGURE 3 Output power vs load resistance under different wind speeds for the proposed 2-DOF GPEH with a secondary beam of the length (A) $H = 100$ mm, (B) $H = 120$ mm, (C) $H = 140$ mm and (D) for the conventional 1-DOF GPEH. The secondary beam is always mounted at a distance of $0.5D$ from the bluff body [Colour figure can be viewed at wileyonlinelibrary.com]

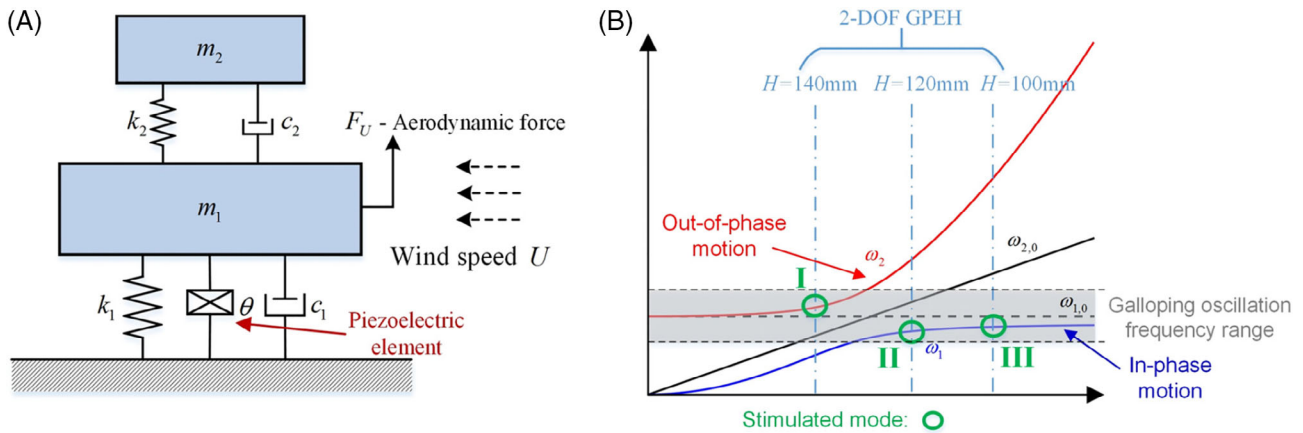


FIGURE 4 (A) Schematic of the 2-DOF GPEH modelled with lumped parameters, (B) the relationship between the natural frequencies of the coupled 2-DOF system and the natural frequencies of the two standalone systems. The red line represents ω_2 , the blue line represents ω_1 , the black solid line represents $\omega_{2,0}$ and the black dashed line represents $\omega_{1,0}$ [Colour figure can be viewed at wileyonlinelibrary.com]

second vibration mode corresponds to the out-of-phase motion, it can be deduced that the reaction force from the secondary system will neutralize the external aerodynamic force applied onto the primary system. Therefore, the vibration intensity of the primary system will be decreased. And the energy output from the piezoelectric element attached to the primary system will be consequently reduced. In contrast, when $\omega_{2,0}$ is tuned larger than $\omega_{1,0}$, the first vibration mode might be dominant. As known that for the first vibration mode, the secondary system has an in-phase motion. The reaction force from the secondary system is in phase with the external aerodynamic force applied onto the primary system. Hence, it can be easily deduced that the vibration intensity of the primary system will be enhanced in this case. In summary, the first in-phase mode will benefit the energy harvesting capacity, while the second out-of-phase mode will deteriorate it. However, it is worth mentioning that the above analysis is just a qualitative deduction and the intersection point at $\omega_{1,0} = \omega_{2,0}$ in Figure 4(B) might not be an accurate criterion to predict whether the first or the second vibration mode plays the dominant role. A more rigorous mathematical derivation is required but not presented here.

From the above qualitative analysis, it is speculated that the two configurations $H = 100$ mm and 120 mm satisfy the condition of stimulating the first in-phase mode, while the configuration of $H = 140$ mm complies with the condition for which the second out-of-phase mode plays the dominant role. To validate this speculation, Figure 5 shows the steady-state time responses of the three configurations of 2-DOF GPEH and the 1-DOF GPEH. The corresponding frequency spectra are also presented using Fast Fourier transform (FFT). It can be known from Figure 5(D) that the natural frequency (ie, $\omega_{1,0}$) of the 1-DOF GPEH is about 9.959 Hz. For the

2-DOF GPEH, how to identify which vibration mode is activated has already been illustrated in Figure 4(B): just compare the vibration frequencies of the 2-DOF GPEH with that of the 1-DOF GPEH. When the vibration frequency is lower than 9.959 Hz (ie, $\omega_{1,0}$), it indicates that the fundamental vibration mode of the 2-DOF GPEH is activated. Otherwise, if the vibration frequency is higher than 9.959 Hz, it implies that second-order vibration mode of the 2-DOF GPEH is activated.

From Figure 5(A) and (B), we can find that the dominant frequencies of both configurations are smaller than 9.959 Hz, which implies that they are the first natural frequencies (ie, ω_1) of the two configurations. In particular, we can note that the first natural frequency ($\omega_1 = 7.441$ Hz) of the configuration $H = 120$ mm is smaller than that ($\omega_1 = 8.281$ Hz) of the configuration $H = 100$ mm. This conforms to the theory of dynamics and vibration and the mechanism can be understood from the sketch presented in Figure 4(B): the configurations of Figure 5(A) and (B) correspond to the circle remarks annotated by II and III, respectively. Using the above theory, the in-phase mode motion explains the improvements observed in the configuration $H = 100$ mm and $H = 120$ mm. From Figure 5(C), we can note that the dominant frequency of the configuration $H = 140$ mm is 10.165 Hz which is larger than 9.959 Hz. This undoubtedly indicates that rather than the first mode, the second mode of the configuration $H = 140$ mm is stimulated: the configuration of Figure 5(C) corresponds to the circle remark annotated by I in Figure 4(B). Thus, we can use the out-of-phase motion theory to explain why the performance of the configuration $H = 140$ mm is deteriorated. In addition, from Figure 5(A)–(D), we can note that the dominant frequencies of the dynamic responses of all the configurations of 2-DOF

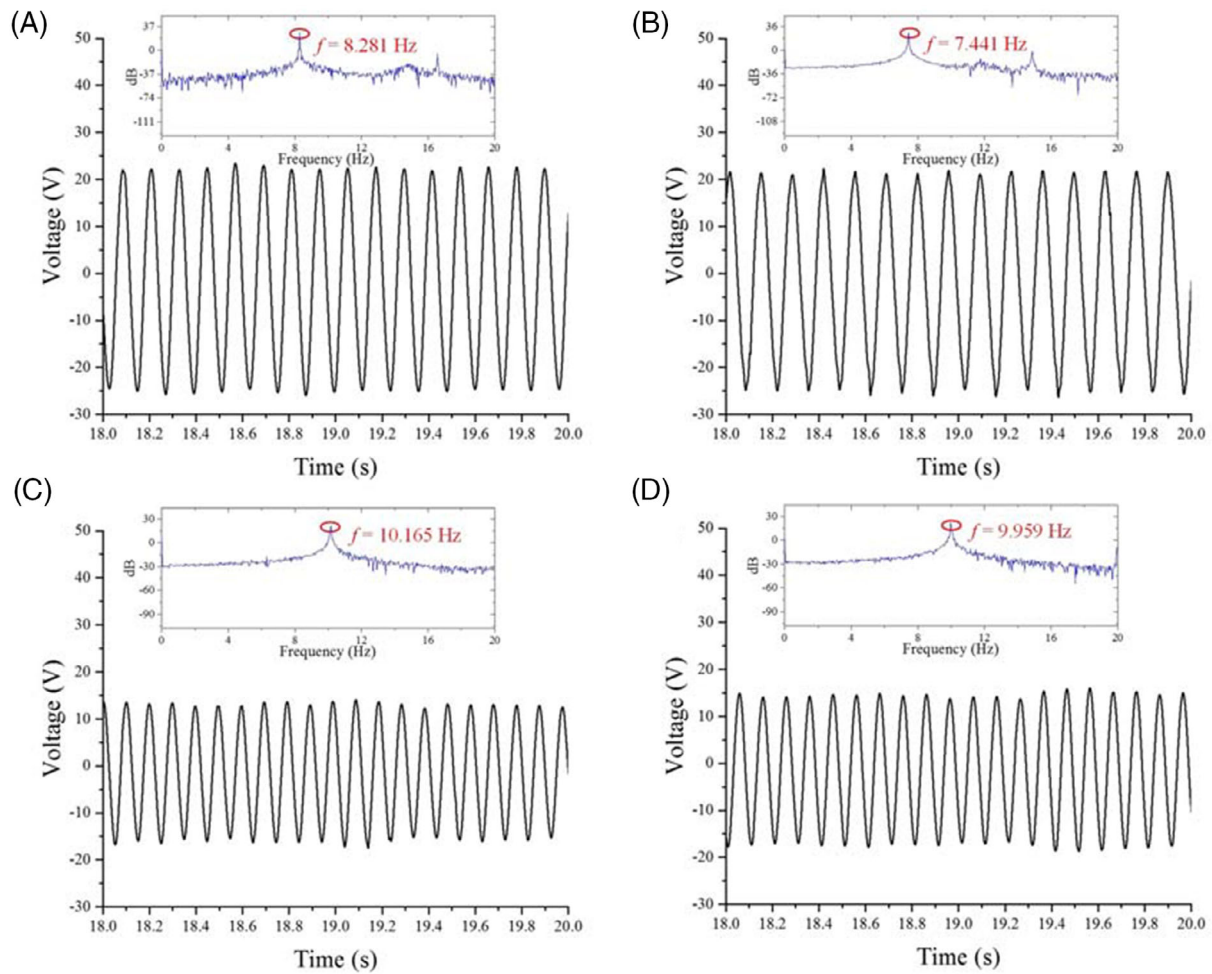


FIGURE 5 Steady-state time histories of the voltage output and the corresponding frequency spectra for (A) 2-DOF GPEH with secondary beam length of 100 mm, (B) 2-DOF GPEH with secondary beam length of 120 mm, (C) 2-DOF GPEH with secondary beam length of 140 mm, (D) 1-DOF GPEH. The load resistance R is fixed at 500 k Ω [Colour figure can be viewed at wileyonlinelibrary.com]

GPEH do not deviate far away from the natural frequency of the 1-DOF GPEH, which implies that the primary system plays the dominant role. Because the primary system remains untouched in the experiment, this explains why the experimental results show that the optimal resistances seem to be the same for all the configurations of the 2-DOF GPEH and the 1-DOF GPEH.

4 | CONCLUSIONS

In conclusion, this paper has proposed a 2-DOF galloping-based piezoelectric energy harvester. Experiments have been conducted to investigate the effects of the secondary beam length and the mounting position on the energy harvesting performance in terms of the cut-in wind speed and the power output amplitude. It has been observed that the cut-in wind speed can be reduced due to the existence of the secondary beam. Moreover, it has been found that the first or the second vibration mode of

the coupled 2-DOF system may be stimulated by tuning the secondary beam length. Since the first vibration mode corresponds to the in-phase motion, when the first vibration mode is stimulated, the power output from the 2-DOF GPEH is speculated to be improved. The example of a well-tuned 2-DOF GPEH with the secondary beam length of 100 mm demonstrates an increase for about 111.1% as compared to the 1-DOF GPEH in terms of the power output. In contrast, if the second vibration mode which corresponds to the out-of-phase motion is stimulated, the power output from the 2-DOF GPEH is speculated to be reduced. The example of a badly tuned 2-DOF GPEH with the secondary beam length of 140 mm demonstrates a 22.2% reduction in the power output. A frequency spectra analysis based on the time history responses of the 2-DOF GPEH validates the theoretical speculations. Regarding the mounting position of the secondary beam, it has been revealed that with the increase of the distance between the secondary beam and the bluff body, the effect of the secondary beam on the

performance of the 2-DOF GPEH is weakened: the reduction of the cut-in wind speed is decreased and the improvement of the power output is also decreased.

ACKNOWLEDGEMENTS

This work was supported by National Natural Science Foundation of China (grant no. 51977196) and the financial support provided by the China Scholarship Council and the University of Auckland Joint Scholarship

NOMENCLATURE

H	Secondary beam length
D	Side length of the cross-section of the bluff body
U	Wind speed
m_1	Primary DOF mass, equivalent mass of the host beam and the bluff body
m_2	Secondary DOF mass, equivalent mass of the secondary beam and the tip mass
k_1	Primary DOF stiffness, equivalent stiffness of the host beam
k_2	Secondary DOF stiffness, equivalent stiffness of the secondary beam
μ	Mass ratio, $\mu = m_2/m_1$
R	Load resistance
$\omega_{1,0}$	Natural frequency of the primary DOF, $\omega_{1,0} = \sqrt{k_1/m_1}$
$\omega_{2,0}$	Natural frequency of the secondary DOF, $\omega_{2,0} = \sqrt{k_2/m_2}$
ω_1	Fundamental natural frequency of the coupled 2-DOF system, that is, 2-DOF GPEH
ω_2	Second natural frequency of the coupled 2-DOF system, that is, 2-DOF GPEH

ORCID

Guobiao Hu  <https://orcid.org/0000-0002-1288-7564>

Junlei Wang  <https://orcid.org/0000-0003-4453-0946>

Liya Zhao  <https://orcid.org/0000-0002-6229-4871>

Lihua Tang  <https://orcid.org/0000-0001-9031-4190>

REFERENCES

- Zhang M, Hu G, Wang J. Bluff body with built-in piezoelectric cantilever for flow-induced energy harvesting. *Int J Energy Res*. 2020;44(5):3762-3777.
- Du Y, Zhou S, Jing X, Peng Y, Wu H, Kwok N. Damage detection techniques for wind turbine blades: a review. *Mech Syst Signal Process*. 2020;141:106445.
- Ding L, Yang L, Yang Z, Zhang L, Wu C, Yan B. Performance improvement of aeroelastic energy harvesters with two symmetrical fin-shaped rods. *J Wind Eng Ind Aerodyn*. 2020;196:104051.
- Hu G, Wang J, Su Z, Li G, Peng H, Kwok K. Performance evaluation of twin piezoelectric wind energy harvesters under mutual interference. *Appl Phys Lett*. 2019;115(7):073901.
- Huang D, Zhou S, Yang Z. Resonance mechanism of nonlinear vibrational multistable energy harvesters under narrow-band stochastic parametric excitations. *Complexity*. 2019;2019:1-20.
- Wang J, Geng L, Ding L, Zhu H, Yurchenko D. The state-of-the-art review on energy harvesting from flow-induced vibrations. *Appl Energy*. 2020;267:114902.
- Wang J, Gu S, Zhang C, et al. Hybrid wind energy scavenging by coupling vortex-induced vibrations and galloping. *Energy Convers Manage*. 2020;213:112835.
- Hu G, Tse KT, Kwok KCS, Song J, Lyu Y. Aerodynamic modification to a circular cylinder to enhance the piezoelectric wind energy harvesting. *Appl Phys Lett*. 2016;109(19):193902.
- Bibo A, Daqaq M. On the optimal performance and universal design curves of galloping energy harvesters. *Appl Phys Lett*. 2014;104(2):023901.
- Gao M, Cong J, Xiao J, et al. Dynamic modeling and experimental investigation of self-powered sensor nodes for freight rail transport. *Appl Energy*. 2020;257:113969.
- Zhao L-C, Zou H-X, Yan G, et al. A water-proof magnetically coupled piezoelectric-electromagnetic hybrid wind energy harvester. *Appl Energy*. 2019;239:735-746.
- Zhu H, Li G, Wang J. Flow-induced vibration of a circular cylinder with splitter plates placed upstream and downstream individually and simultaneously. *Appl Ocean Res*. 2020;97:102084.
- Zhu H, Liu W, Zhou T. Direct numerical simulation of the wake adjustment and hydrodynamic characteristics of a circular cylinder symmetrically attached with fin-shaped strips. *Ocean Eng*. 2020;195:106756.
- Xu W, Ji C, Sun H, Ding W, Bernitsas MM. Flow-induced vibration of two elastically mounted tandem cylinders in cross-flow at subcritical Reynolds numbers. *Ocean Eng*. 2019;173:375-387.
- Ma Y, Luan Y, Xu W. Hydrodynamic features of three equally spaced, long flexible cylinders undergoing flow-induced vibration. *Eur J Mech-B/Fluids*. 2020;79:386-400.
- Hu G, Kwok K. Predicting wind pressures around circular cylinders using machine learning techniques. *J Wind Eng Ind Aerodyn*. 2020;198:104099.
- Hu G, Tse K, Wei M, Naseer R, Abdelkefi A, Kwok K. Experimental investigation on the efficiency of circular cylinder-based wind energy harvester with different rod-shaped attachments. *Appl Energy*. 2018;226:682-689.
- Wang J, Tang L, Zhao L, Zhang Z. Efficiency investigation on energy harvesting from airflows in hvac system based on galloping of isosceles triangle sectioned bluff bodies. *Energy*. 2019;172:1066-1078.
- Yan Z, Wang L, Hajj MR, Yan Z, Sun Y, Tan T. Energy harvesting from iced-conductor inspired wake galloping. *Extreme Mech Lett*. 2020;35:100633.
- Liu F-R, Zhang W-M, Zhao L-C, et al. Performance enhancement of wind energy harvester utilizing wake flow induced by double upstream flat-plates. *Appl Energy*. 2020;257:114034.
- Eugeni M, Elahi H, Fune F, et al. Numerical and experimental investigation of piezoelectric energy harvester based on flag-flutter. *Aerospace Sci Technol*. 2020;97:105634.
- Wang J, Hu G, Su Z, et al. A cross-coupled dual-beam for multi-directional energy harvesting from vortex induced vibrations. *Smart Mater Struct*. 2019;28(12):12LT02.
- Zhu H, Yao J. Numerical evaluation of passive control of viv by small control rods. *Appl Ocean Res*. 2015;51:93-116.

24. Zhu H, Yao J, Ma Y, Zhao H, Tang Y. Simultaneous CFD evaluation of vortex suppression using smaller control cylinders. *J Fluids Struct.* 2015;57:66-80.
25. Zou Q, Ding L, Wang H, Wang J, Zhang L. Two-degree-of-freedom flow-induced vibration of a rotating circular cylinder. *Ocean Eng.* 2019;191:106505.
26. Arroyo E, Badel A, Formosa F, Wu Y, Qiu J. Comparison of electromagnetic and piezoelectric vibration energy harvesters: model and experiments. *Sens Actuat A: Phys.* 2012;183:148-156.
27. Ma H, Yan B. Nonlinear damping and mass effects of electromagnetic shunt damping for enhanced nonlinear vibration isolation. *Mech Syst Signal Process.* 2021;146:107010.
28. Yan B, Ma H, Zhang L, Zheng W, Wang K, Wu C. A bistable vibration isolator with nonlinear electromagnetic shunt damping. *Mech Syst Signal Process.* 2020;136:106504.
29. Zhao L-C, Zou H-X, Gao Q-H, et al. Magnetically modulated orbit for human motion energy harvesting. *Appl Phys Lett.* 2019;115(26):263902.
30. Chen G, Tang L, Yang Z, Tao K, Yu Z. An electret-based thermoacoustic-electrostatic power generator. *Int J Energy Res.* 2020;44(3):2298-2305.
31. Zhang L, Meng B, Xia Y, et al. Galloping triboelectric nanogenerator for energy harvesting under low wind speed. *Nano Energy.* 2020;70:104477.
32. Fang S, Wang S, Zhou S, Yang Z, Liao W-H. Exploiting the advantages of the centrifugal softening effect in rotational impact energy harvesting. *Appl Phys Lett.* 2020;116(6):063903.
33. Yang Y, Zhao L, Tang L. Comparative study of tip cross-sections for efficient galloping energy harvesting. *Appl Phys Lett.* 2013;102(6):064105.
34. Fang S, Fu X, Liao W-H. Asymmetric plucking bistable energy harvester: modeling and experimental validation. *J Sound Vib.* 2019;459:114852.
35. Fang S, Wang S, Miao G, et al. Comprehensive theoretical and experimental investigation of the rotational impact energy harvester with the centrifugal softening effect. *Nonlinear Dynam.* 2020.101(1):123-152.
36. Zou H-X, Zhao L-C, Gao Q-H, et al. Mechanical modulations for enhancing energy harvesting: principles, methods and applications. *Appl Energy.* 2019;255:113871.
37. Huang D, Zhou S, Han Q, Litak G. Response analysis of the nonlinear vibration energy harvester with an uncertain parameter. *Proceedings of the Institution of Mechanical Engineers, Part K: Journal of Multi-Body Dynamics.* 2019;234(2):393-407.
38. Zhou S, Zuo L. Nonlinear dynamic analysis of asymmetric tristable energy harvesters for enhanced energy harvesting. *Commun Nonlinear Sci Numer Simul.* 2018;61:271-284.
39. Lu Z, Gu D, Ding H, Lacarbonara W, Chen L. Nonlinear vibration isolation via a circular ring. *Mech Syst Signal Process.* 2020;136:106490.
40. Fang S, Fu X, Du X, Liao W-H. A music-box-like extended rotational plucking energy harvester with multiple piezoelectric cantilevers. *Appl Phys Lett.* 2019;114(23):233902.
41. Sirohi J, Mahadik R. Harvesting wind energy using a galloping piezoelectric beam. *J Vibr Acoust.* 2012;134(1):011009.
42. Barrero-Gil A, Alonso G, Sanz-Andres A. Energy harvesting from transverse galloping. *J Sound Vib.* 2010;329(14):2873-2883.
43. Tang L, Zhao L, Yang Y, Lefeuvre E. Equivalent circuit representation and analysis of galloping-based wind energy harvesting. *IEEE/ASME Trans Mechatron.* 2014;20(2):834-844.
44. Wang J, Tang L, Zhao L, Hu G, Song R, Xu K. Equivalent circuit representation of a vortex-induced vibration-based energy harvester using a semi-empirical lumped parameter approach. *Int J Energy Res.* 2020;44(6):4516-4528.
45. Bibo A, Alhadidi AH, Daqaq MF. Exploiting a nonlinear restoring force to improve the performance of flow energy harvesters. *J Appl Phys.* 2015;117(4):045103.
46. Yang K, Wang J, Yurchenko D. A double-beam piezo-magneto-elastic wind energy harvester for improving the galloping-based energy harvesting. *Appl Phys Lett.* 2019;115(19):193901.
47. Wang J, Geng L, Zhou S, Zhang Z, Lai Z, Yurchenko D. Design, modeling and experiments of broadband tristable galloping piezoelectric energy harvester. *Acta Mech Sin.* 2020;36:592-605.
48. Wang J, Geng L, Yang K, Zhao L, Wang F, Yurchenko D. Dynamics of the double-beam piezo-magneto-elastic nonlinear wind energy harvester exhibiting galloping-based vibration. *Nonlinear Dynam.* 2020;100:1963-1983.
49. He X, Yang X, Jiang S. Enhancement of wind energy harvesting by interaction between vortex-induced vibration and galloping. *Appl Phys Lett.* 2018;112(3):033901.
50. Wang J, Zhou S, Zhang Z, Yurchenko D. High-performance piezoelectric wind energy harvester with y-shaped attachments. *Energy Convers Manage.* 2019;181:645-652.
51. Zhao L, Tang L, Yang Y. Enhanced piezoelectric galloping energy harvesting using 2 degree-of-freedom cut-out cantilever with magnetic interaction. *Jpn J Appl Phys.* 2014;53(6):060302.
52. Sun W, Guo F, Seok J. Development of a novel vibro-wind galloping energy harvester with high power density incorporated with a nested bluff-body structure. *Energy Convers Manage.* 2019;197:111880.
53. Lan C, Tang L, Hu G, Qin W. Dynamics and performance of a two degree-of-freedom galloping-based piezoelectric energy harvester. *Smart Mater Struct.* 2019;28(4):045018.
54. Xiong L, Tang L, Mace BR. Internal resonance with commensurability induced by an auxiliary oscillator for broadband energy harvesting. *Appl Phys Lett.* 2016;108(20):203901.
55. Hu G, Tang L, Das R. Metamaterial-inspired piezoelectric system with dual functionalities: energy harvesting and vibration suppression. *Proc SPIE.* 10164. Portland, OR: Society of Photo-Optical Instrumentation Engineers (SPIE); 2017.
56. Abdelkefi A, Najjar F, Nayfeh A, Ayed SB. An energy harvester using piezoelectric cantilever beams undergoing coupled bending-torsion vibrations. *Smart Mater Struct.* 2011;20(11):115007.

How to cite this article: Hu G, Wang J, Qiao H, Zhao L, Li Z, Tang L. An experimental study of a two-degree-of-freedom galloping energy harvester. *Int J Energy Res.* 2020;1-9. <https://doi.org/10.1002/er.5878>